Observations of Polarity Reversal in Shoaling Nonlinear Internal Waves

E. L. SHROYER, J. N. MOUM, AND J. D. NASH

College of Oceanic and Atmospheric Sciences, Oregon State University, Corvallis, Oregon

(Manuscript received 20 November 2007, in final form 28 March 2008)

ABSTRACT

Observations off the New Jersey coast document the shoaling of three groups of nonlinear internal waves of depression over 35 km across the shelf. Each wave group experienced changing background conditions along its shoreward transit. Despite different wave environments, a clear pattern emerges. Nearly symmetric waves propagating into shallow water develop an asymmetric shape; in the wave reference frame, the leading edge accelerates causing the front face to broaden while the trailing face remains steep. This trend continues until the front edge and face of the leading depression wave become unidentifiable and a near-bottom elevation wave emerges, formed from the trailing face of the initial depression wave and the leading face of the following wave. The transition from depression to elevation waves is diagnosed by the integrated wave vorticity, which changes sign as the wave's polarity changes sign. This transition is predicted by the sign change of the coefficient of the nonlinear term in the KdV equation, when evaluated using observed profiles of stratification and velocity.

1. Introduction

The role of nonlinear internal waves (NLIWs) in the coastal ocean has been the study of recent investigations, as many processes may be influenced by these waves. In addition to the potential transport of sediment (Bogucki et al. 1997), nutrients, and biota (Pineda 1994; Lamb 1997, 2003), these waves may have a profound effect on human activities such as offshore drilling operations and waste disposal (Osborne and Burch 1980). NLIWs are often associated with large turbulent mixing events (Klymak and Moum 2003; Moum et al. 2003, 2007) and are thought to be an important link in energy dissipation from the barotropic tide (e.g., Sandstrom and Elliott 1984; Sandstrom and Oakey 1995). For these reasons, emphasis has been placed on understanding the formation, evolution, and demise of nonlinear internal waves. In this paper we attempt to address the latter part of this story by documenting the shoaling of three groups of nonlinear internal waves of depression.

A pycnocline located near the surface supports waves of depression; however, in shallow water or winter stratification, the pycnocline is often located closer to the bottom than the surface, supporting waves of elevation. As a depression wave train shoals, the wave group encounters an increasingly shallow water column. If the pycnocline maintains a constant depth across the shelf, there exists the possibility of a point at which the depression wave group will transition into elevation waves. While field observations documenting reversal of wave polarity are scarce, some modeling and laboratory studies have been designed with the intent of elucidating the evolution process through a critical point, where the first-order nonlinear term vanishes and the fluid shifts from depression to elevation wave favorable (Helfrich et al. 1984; Helfrich and Melville 1986; Liu et al. 1998; Zhao et al. 2003; Grimshaw et al. 2004; Vlasenko and Stashchuk 2007). Most of these studies rely on weakly nonlinear theory to describe the evolution of the shoaling wave; however, Vlasenko and Stashchuk (2007) employ a fully nonlinear model. In general, as the modeled soliton approaches the critical point a dispersive wave tail forms consisting of elevation and depression waves, while at the same time an asymmetry in the lead wave develops with the front edge traveling faster than the rear edge. Eventually the lead wave is destroyed, and an elevation wave emerges from the dispersive tail.

The exact positions where the various studies refer to the destruction of the lead depression wave and emergence of elevation waves differ. For example, Liu et al. [1998; using a modified version of the extended

Corresponding author address: E. L. Shroyer, College of Oceanic and Atmospheric Sciences, Oregon State University, 104 Ocean Admin Bldg., Corvallis, OR 97331–5503.
E-mail: eshroyer@coas.oregonstate.edu

DOI: 10.1175/2008JPO3953.1

Korteweg–de Vries (eKdV) equation] note the creation of an elevation wave behind the lead depression wave well in advance of the critical point in accordance with Vlasenko and Stashchuk (2007). However, whereas Liu et al. (1998) continue to refer to the lead depression disturbance as a wave well beyond the critical point, Vlasenko and Stashchuk (2007) refer to the disturbance as a depressed pycnocline and claim conversion happens prior to the critical point. Despite the different terminologies, a comparison between Fig. 10 in Liu et al. (1998) and Fig. 4 in Vlasenko and Stashchuk (2007) reveals a similar development in the shoaling wave. This similarity is perhaps even more surprising because of the significant differences in both the models used and their initialization (e.g., wave amplitude, stratification, and bottom slope).

In a separate study using a fully nonlinear model, Vlasenko and Hutter (2002) found that a shoaling depression wave may collapse into a bottom-trapped, elevated mass of fluid, resembling an undular bore, after wave breaking. The authors noted two distinct cases of wave shoaling. The first was controlled primarily by dispersion, resulting in a long wave of depression followed by a dispersive wave train, qualitatively similar to results from weakly nonlinear models. The second case was that nonlinearity dominated wave dynamics, resulting in wave breaking. The rear face of the shoaling wave steepened until a kinematic instability formed, where particle speeds exceeded the local wave speed. The authors established a breaking criterion for the waves, which is both a confirmation and extension of the criterion established by Helfrich and Melville (1986) for steeper slopes.

This paper examines the shoaling process of three wave trains across the New Jersey shelf. In section 2 the concept of a critical point is reviewed. The experimental design is outlined in section 3. A description of wave properties and background conditions is given in section 4. The shoaling process of each wave train is examined in detail in section 5, and concluding remarks are presented in section 6.

2. Definition: The critical point ($\alpha = 0$)

Nonlinear internal waves observed in geophysical fluids do not generally satisfy assumptions made in weakly nonlinear theory. However, the soliton solution to the KdV equation can be used to illustrate the existence of a critical point. For a KdV soliton, the wavelength, λ, is related to the amplitude by

$$\lambda^2 \eta_0 = 12 \frac{\beta}{\alpha}. \tag{1}$$

The coefficients of the nonlinear and dispersive terms, α and β, depend on the linear vertical structure function, ϕ, and linear wave speed, c_0, as follows:

$$\alpha = \frac{3 \int_{-H}^{0} (c_0 - U)^2 \phi_z^3 dz}{2 \int_{-H}^{0} (c_0 - U) \phi_z^2 dz}, \tag{2}$$

$$\beta = \frac{\int_{-H}^{0} (c_0 - U)^2 \phi^2 dz}{2 \int_{-H}^{0} (c_0 - U) \phi_z^2 dz}. \tag{3}$$

As long as c_0 is everywhere greater than U, oceanic conditions control the polarity of the soliton through the sign of the coefficient, α, as evident in relation (1). In a two-layer fluid without background shear, the transition between $\eta_0 > 0$ and $\eta_0 < 0$ occurs at a critical point (defined as $\alpha = 0$) when $h_1 = h_2$, where h_1 and h_2 are the depth of the upper and lower layer, respectively. This result may be extended to include an upper- (U_1) and lower-layer velocity (U_2), which provides a simple interpretation of the effect of background shear on wave transition (4):

$$\frac{h_1}{h_2} = \frac{c_0 - U_1}{c_0 - U_2}. \tag{4}$$

As an example, consider the case where U_1 is in the direction of wave propagation (i.e., toward shallower water), while U_2 travels in the opposite direction (i.e., $U_2 < 0$). In this case, the ratio on the rhs of (4) is less than 1, and the wave will reach the critical point before $h_1 = h_2$. The transition will be delayed if the ratio on the rhs is greater than 1. While this development is simple, it serves as a useful illustration of the effect background shear has on the location of the critical point. The parameters, α and β, may be computed numerically from (2) and (3) for a fully stratified flow with background shear. In section 5, we test the efficacy of using α to define wave polarity by comparison to an observational diagnostic.

In reality, higher-order or fully nonlinear theories are needed to describe the transition across a critical point, since by definition the solitary wave does not exist when $\alpha = 0$. Including a cubic nonlinear term in the equation allows for the development of multiple critical points associated with both the quadratic and cubic nonlinear coefficients. Grimshaw et al. (2004) provide a useful, more detailed description of the possible wave transformation scenarios using this expanded theory.

3. Experimental details

Shipboard measurements on the R/V *Oceanus* were conducted off the coast of New Jersey in conjunction

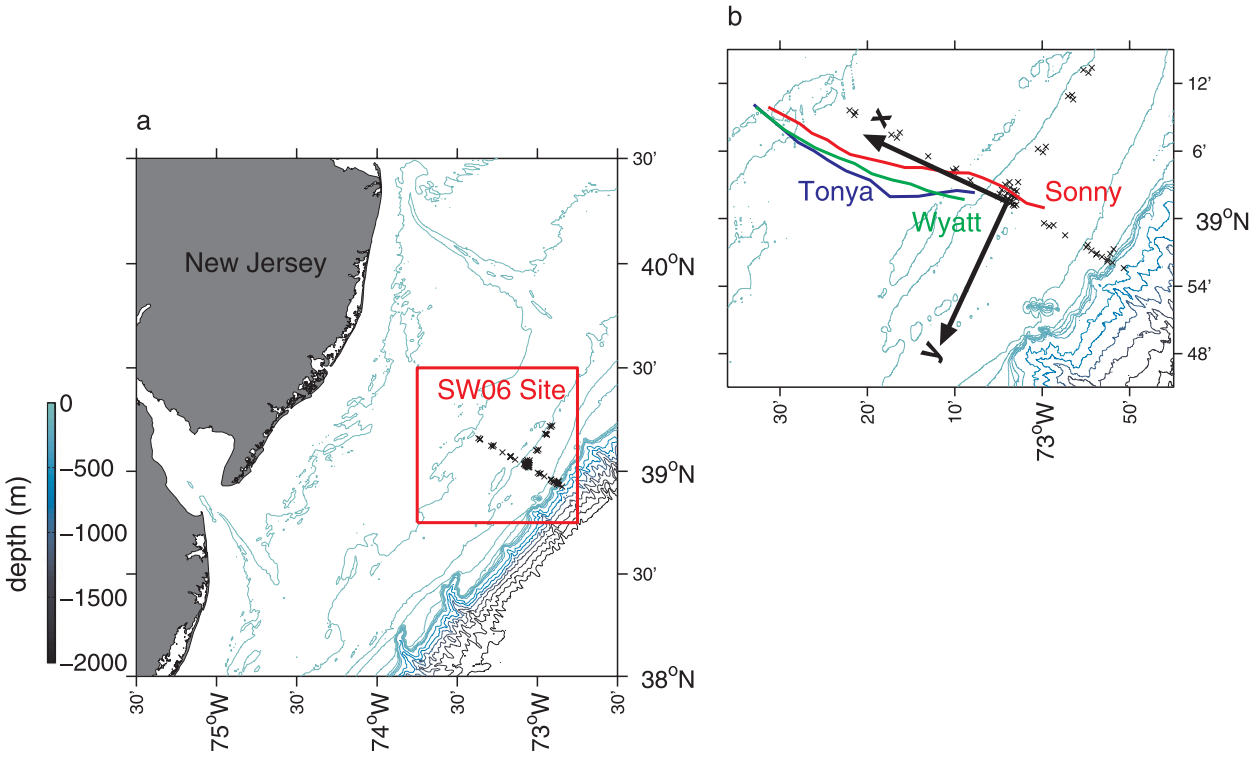

FIG. 1. (a) SW06 site and bathymetry. Black Xs indicate locations of SW06 moorings. (b) Ship transects following *Wave Sonny* (red), *Wave Tonya* (blue), and *Wave Wyatt* (green). The waves were tracked perpendicular to wave fronts, determined visually and from the ship's radar. The wave reference frame is rotated into the mean direction of wave propagation, and the origin positioned at the intersection of the T-shaped mooring array (mooring SW30).

with the Nonlinear Internal Wave Initiative/Shallow Water '06 Experiment (NLIWI/SW06) in August 2006 (Tang and et al., 2007). Site location and mooring positions are indicated in Fig. 1; although the data presented here are solely from shipboard observations, mooring locations are shown for future reference. NLIWs were located and tracked using a range of shipboard acoustics. High-resolution echo sounder images provided a qualitative view of the wave structure and were useful in tracking disturbances in real time. Velocity data were obtained using both a hull-mounted 300-kHz ADCP and a side-mounted 1200-kHz ADCP. The setup permitted velocity measurements from ~10 m above the sea floor to within 3 m of the surface. Depending on wind speed and direction, the ship's X-band radar provided a clear picture of wave orientation; these images along with visual sightings of wave fronts helped us to make our crossings perpendicular to wave fronts.

Once a wave train was identified, the wave group was transited at a high speed (3–4 m s^{-1}), providing a relatively undistorted view of the waves. The ship was then positioned ahead of the waves and held semistationary as microstructure measurements of density (σ_θ) and turbulence dissipation rate (ϵ) were made using the Chameleon profiler (Moum et al. 1995). On average, five profiles were obtained through a given wave in a train; however, this number varied depending on the disturbance width and the relative ship–wave motion. The ship maintained position as the first few waves of the train propagated past (typically 3–4), then the profiler was recovered and the process repeated. At each station, the profiling period lasted from a half-hour to an hour. This "leapfrog" method continued as the waves propagated onshore, enabling multiple observations of a single evolving wave group to be made over long distances, in some cases in excess of 50 km.

4. Observations

a. Wave properties

During the course of the cruise (~1 month), observations of 27 wave groups were made. Background stratification and shear varied in both time and space, creating heterogeneous conditions for wave groups along their shoreward journey. A naming convention was adopted for bookkeeping purposes. In this paper, we examine the evolution of three wave groups, *Wave Sonny*, *Wave Tonya*, and *Wave Wyatt*, first observed at

2000 UTC 18 August 2006, 1400 UTC 20 August 2006, and 0800 UTC 22 August 2006, respectively. In each case, waves were followed onshore more than 35 km (~14 h), over which time at least 10 Chameleon profiling time series were made. These three wave groups are unique in that they provide clear observational evidence of polarity reversal. The other 24 wave groups were either not tracked as far inshore (so that the critical point for wave transition was not captured), or the waves were of smaller amplitude (so that the wave signal deteriorated before transition could be observed). As a result, we focus the following analysis on the three wave packets: *Sonny*, *Tonya*, and *Wyatt*.

The ship transects following these waves are shown in Fig. 1; except for small deviations primarily required to avoid mooring positions, the waves were tracked perpendicular to wave fronts. Distances along the wave path are defined using the axes shown in black. The positive x axis is oriented in the mean direction of wave propagation, and the origin is defined at mooring SW30, located at the intersection of the T-shaped array.

The changes in the vertical scale, horizontal scale, and wave speed of the lead waves are shown in Fig. 2. The vertical scale of the wave, A, is an estimate of the maximum displacement of scattering layers, which correspond closely to density surfaces; here we define waves of depression as having negative A. The A is equivalent to the amplitude, η_0, for a KdV soliton (section 2). The horizontal wave scale, L, is an estimate of the total disturbance width, which for a symmetric KdV soliton would correspond to 4λ as defined in section 2. We use A and L as opposed to η_0 and λ because of the highly nonlinear, asymmetric nature of the observed waves. Wave speeds were calculated from the inverse slope of the time–position plot of maximum displacement (Fig. 2c).

Mean wave speeds and propagation direction, as calculated from acoustic backscatter and radar, were 0.74, 0.73, and 0.71 m s^{-1} and 300°, 300°, and 310° for *Sonny*, *Tonya*, and *Wyatt*, respectively. These wave speeds represent the mean over the entire transit period; local phase speeds vary likely due to modulation by the internal tide. *Wave Sonny* initially had a horizontal scale, L, of ~500 m that broadened to over 1300 m prior to transition. *Tonya's* horizontal wave scale increased from 400 to 1200 m, and *Wyatt* displayed the most extreme example of broadening, increasing nearly 5 times from an initial L of 300 m. The amplitude of *Wave Sonny* decreased from $A \approx -12$ to $A \approx -6$ m prior to transition. *Waves Tonya* and *Wyatt* experienced rapid, extreme changes in amplitude, in which A nearly doubled in magnitude for a short distance. These anomalies (denoted by circles in Fig. 2a) are associated with potential wave interactions; a more detailed analysis of these interactions is the focus of a separate study. These deviations are superimposed on a gradual decreasing trend from amplitudes of −10 and −12 m to −5 and −5 m for *Tonya* and *Wyatt*, respectively.

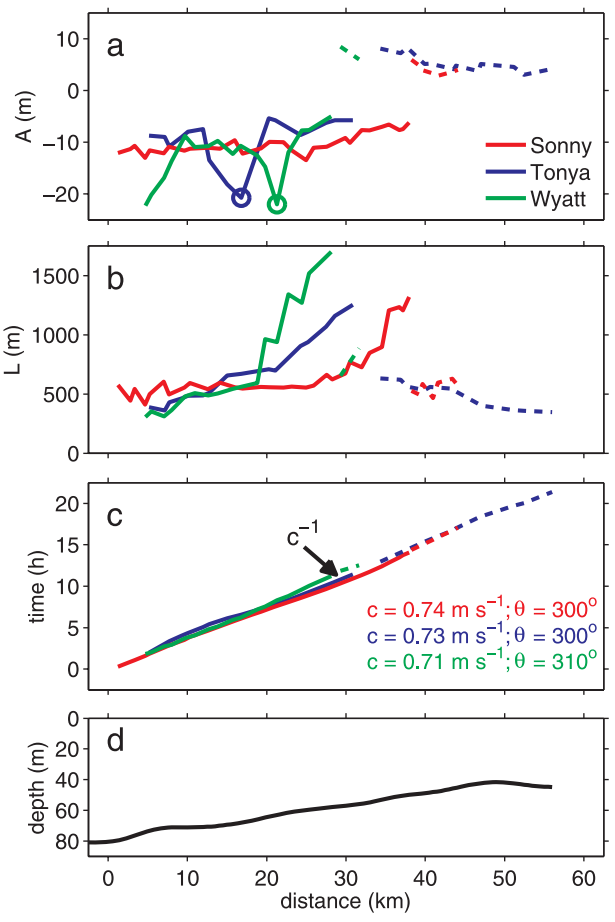

FIG. 2. (a) A, (b) L, and (c) time–position of the leading wave. Here L is a measure of the full disturbance length. Solid lines indicate depression waves, and dashed lines indicate elevation waves. The circles in (a) show locations of wave interactions. Average wave speeds, $c = \Delta x/\Delta t$, and headings are given in (c). The bottom depth is shown in (d).

The signature of the observed waves deteriorated before breaking of the lead elevation wave could be documented. This was possibly due to limitations in our tracking techniques, as very short (50 m) NLIWs of elevation have been observed in the region shoreward of the 30-m isobath (Scotti and Pineda 2004). In particular, the ability to distinguish a small-amplitude, short wave from a moving platform depends on the relative ship to wave speed. Assuming a relative speed of a few meters per second, real-time observations would last for under a minute for a wave with a length of ~100 m. It is also possible that dissipation by bottom friction accounts for the loss of the wave signature.

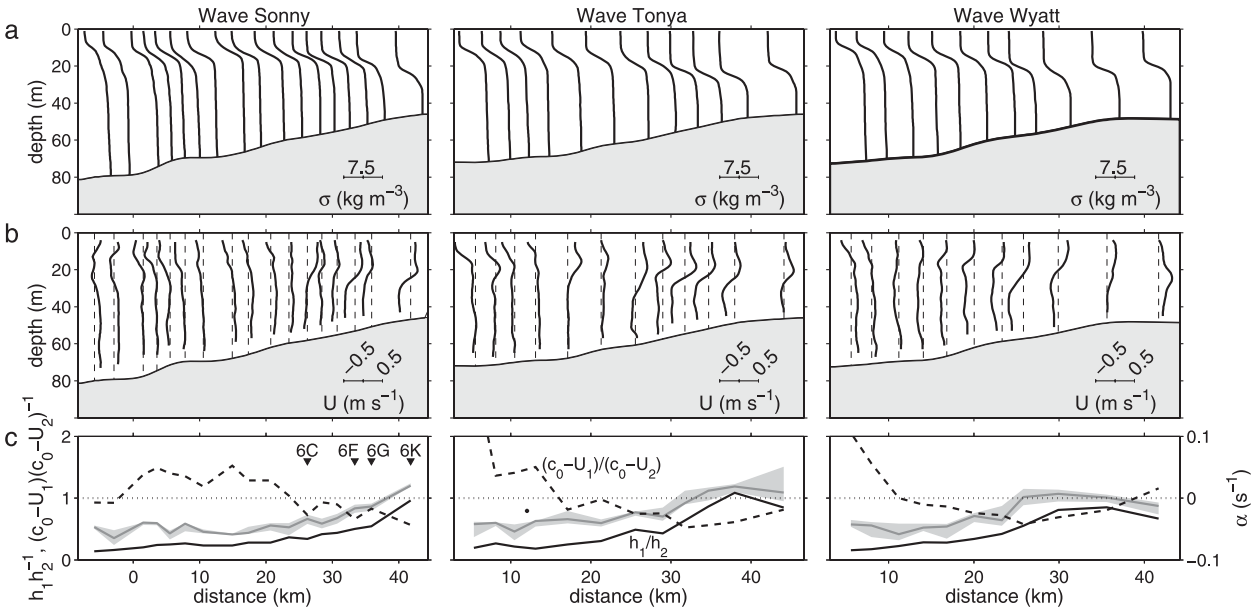

FIG. 3. Profiles of (a) density and (b) background velocity ahead of *Waves Sonny*, *Tonya*, and *Wyatt*. (c) The left axis and corresponding black solid and dashed lines represent the two-layer relation described in (4). The continuous case is represented by the change in sign of α (gray line) corresponding to the right axis. The critical point defined by the two-layer approximation is consistent with the continuous estimate for each wave group. For *Wave Sonny* the critical point occurs at approximately 38 km, and for *Tonya* the critical point occurs near 33 km. For *Wave Wyatt* conditions are more varied, and the fluid alternates from supporting depression waves to elevation waves (~26–36 km) and back again to depression waves. Black triangles located on *Sonny* in (c) refer to positions in Fig. 6 and correspond to transects shown in Fig. 4.

b. *Background conditions: Properties of the waveguide*

Background profiles of density and velocity for *Waves Sonny*, *Tonya*, and *Wyatt* are shown in Fig. 3. Background density is estimated using at least one full depth profile taken prior to the wave's arrival at a given location; if more than one profile was obtained ahead of the wave, the average is used. Background velocity measurements represent a 5-min time average of data taken ahead of the wave; for calculation of α, values are extrapolated to the surface and at depth using a constant velocity. In all cases the pycnocline depth (Fig. 3a) increased as the water depth decreased, hinting at the development of a critical point. A reversal in the background shear (Fig. 3b) was apparent during each wave's shoreward transit time. Since the wave transit times exceeded the M_2 tidal period, tidal motions are certainly aliased into this signal. The fluid may be approximated as two layers using the maximum value of buoyancy frequency to distinguish the interface. Average values of background velocity were used to compute the ratio in (4) shown in Fig. 3c (black lines, left axis). When $h_1h_2^{-1}$ (solid black line) $\geq (c_0 - U_1)(c_0 - U_2)^{-1}$ (dashed black line), the fluid transitioned to elevation wave favorable. While we base the location of the critical point on $\alpha = 0$ (gray line), computed using observed profiles of density and velocity, we note that the two-layer approximation is consistent with this fully stratified, sheared calculation [i.e., $\alpha = 0$ occurs when $h_1h_2^{-1} = (c_0 - U_1)(c_0 - U_2)^{-1}$]. The two-layer approximation is useful in distinguishing the consequence of the background shear on the location of the critical point. The shaded gray regions surrounding the darker gray lines are confidence limits assuming that the depth bin position for both density and velocity is known to within ±2 m.

The exact location of the critical point ($\alpha = 0$) and nature of the waveguide shoreward of this point differed for each wave group. For *Wave Sonny*, the very last profile approached the critical point for a two-layer fluid without shear flow with $h_1h_2^{-1} = 1$, and exceeded the critical point for a shear flow [$h_1h_2^{-1} \geq (c_0 - U_1)(c_0 - U_2)^{-1}$]. Unfortunately, the wave group was poorly defined much past this point, preventing extensive observations in the elevation-friendly environment. In contrast, *Wave Tonya* was followed for a considerable distance after passing through the critical point at around 32.5 km. The background conditions for *Wave Wyatt* were complex, in that the fluid switched from supporting depression waves to elevation waves (~26–36 km) and back again to depression waves. In fact, the waveguide seemed to hover

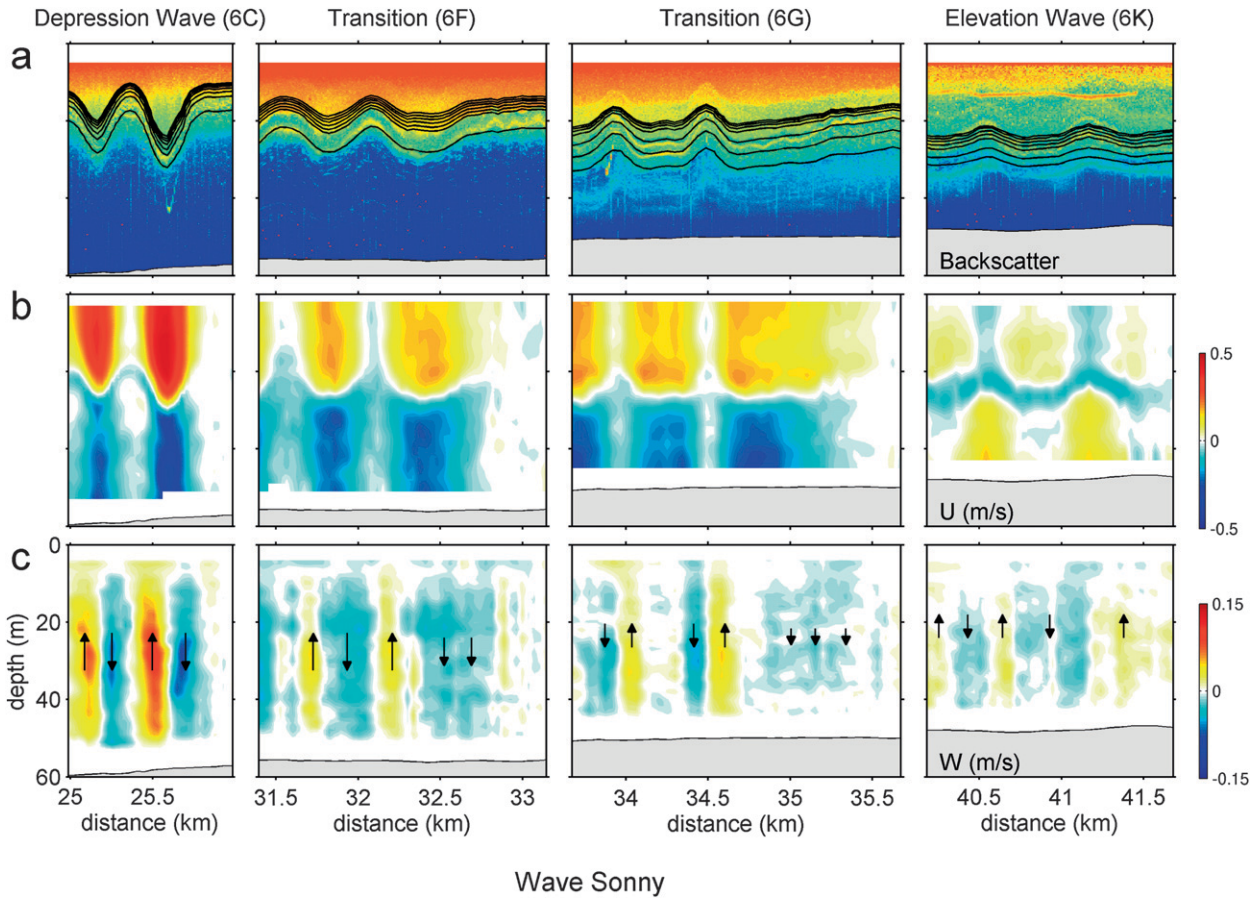

FIG. 4. (a) Acoustic backscatter, (b) horizontal velocity, and (c) vertical velocity shown for four different periods along the propagation path of *Wave Sonny*. The wave is propagating to the right. Isopycnals range from 22.25 to 25.25 kg m^{-3}. Black arrows emphasize downward and upward motions. The relative size of the arrows is representative of the magnitude of the vertical velocity. The wave states (depression, transition, and elevation) correspond to Figs. 6c,f,g,k. These locations are also marked in Fig. 3c.

around the critical point ($\alpha \approx 0$) rather than undergoing a definitive transition.

5. Discussion: Wave shoaling and polarity reversal

Time series showing the evolution of *Wave Sonny* as it developed from a depression wave through transition to an elevation wave, are presented in Fig. 4. These series were taken during semistationary times of shipboard profiling; the time series were converted into distance plots using wave speed. Isopycnals calculated from streamlines, following the method outlined by Moum and Smyth (2006), are contoured in black. The background velocity has been subtracted using the upstream vertical profile mapped onto isopycnals. Initially, the structure of the leading depression wave (Fig. 4, left column) was symmetric. The horizontal velocity reached a maximum speed in excess of 0.45 m s^{-1}, and there was a strong compensating flow at depth. The vertical velocity signature shows a downward velocity at the leading edge and upward motion at the trailing edge of each wave. As the wave shoaled, an asymmetry in the leading wave developed (Fig. 4, middle columns); the front face of the wave broadened and the rear face of the wave remained steep. The maximum horizontal velocity shifted closer to the rear face of the wave; this is similar to the description given by Vlasenko and Hutter (2002). Accompanying the elongation of the leading face and convergent region, the downwelling region became weaker in magnitude but broader in scale while the upward motion present at the steep rear face remained sharp and clearly defined. In the final stage as a leading elevation wave emerged (Fig. 4, right column), an upward pulse preceded a downward pulse of equal magnitude; we take this as a defining characteristic of elevation waves. At this point, maximum horizontal velocities were ~0.13 m s^{-1}, 5 times smaller than the phase speed of the wave. Referring to Fig. 3, the observed appearance of the leading elevation wave at about 40 km is consistent with the transition through the theoretical critical

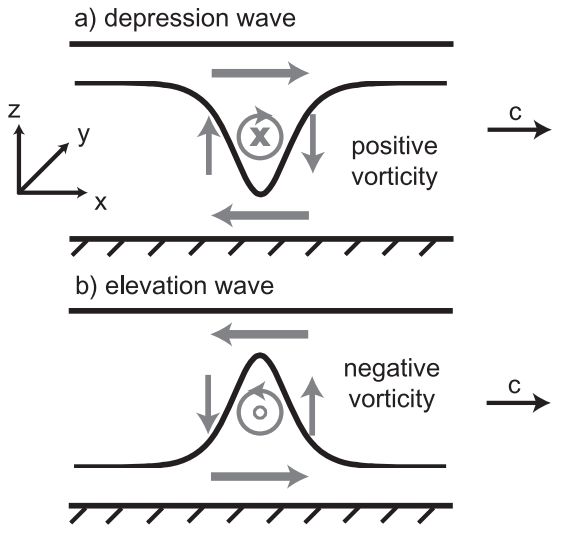

FIG. 5. Schematic illustrating the sign of vorticity for (a) depression and (b) elevation waves.

point at 38 km, as defined by the background conditions alone.

Figure 4 demonstrates that the sign of the vorticity for depression waves is different from that of elevation waves for waves propagating in the same direction. These two cases are clarified in Fig. 5. We employ this distinction as an observational diagnostic, and define the integrated wave vorticity:

$$\Omega_w = \int_{-H}^{0} \omega dz = \int_{-H}^{0} \frac{\partial u_{\text{wave}}}{\partial z} - \frac{\partial w_{\text{wave}}}{\partial x} dz. \qquad (5)$$

For a wave of depression (elevation) propagating in the positive x direction, the integrated wave vorticity is positive (negative). This is a useful characteristic for our purposes, since we follow waves that change sign but not propagation direction. The Ω_w is evaluated for each transect and its change in sign used as a marker for the observed location of the critical point.

The acoustic backscatter series shown in Fig. 6a for *Wave Sonny* provides a means of visualizing the developing wave form. Well-formed depression waves were observed during the earliest stages, when the pycnocline was approximately 15 m in almost 70 m of water (Figs. 6a,b). As the wave shoaled, the leading wave began to form a slight asymmetry (between 30 and 35 km; Figs. 6e,f). This trend became more pronounced as the wave approached the critical point (Figs. 6g–i), after which freely propagating elevation waves emerged (Figs. 6j,k). The sign of the lead wave vorticity in the last two transects is negative (Fig. 6b). The process resembles the transformation described by models (e.g., Liu et al. 1998; Vlasenko and Stashchuk 2007), although as mentioned in section 1, ambiguity exists in defining a precise location for the demise of the lead elevation wave. In these observations the case is further complicated by the difficulty in distinguishing dispersive waves from preexisting wave forms (i.e., observations are the product of several shoaling waves rather than a single soliton). Deciphering the details of the wave train's evolution is complicated by the coarse horizontal resolution of the observations; wave crossings are separated by distances of approximately $5L$. Another source of disparity between the observed and modeled waves arises from differences in the model initializations and observations. In this work, we have chosen to define the observed transition as the location at which the lead wave's velocity signal can no longer be separated from the mean flow (i.e., $\Omega_w = 0$). However, while care was taken to ensure that the R/V *Oceanus* was not prematurely turned on transects, distinguishing the leading edge of a wide ($\sim$2 km), small-amplitude ($<$5 m) wave is somewhat subjective. And yet, the demise of the leading depression wave as defined by $\Omega_w = 0$ was coincident with the transition region as predicted by the change in sign of α from first-order KdV analysis.

The development of the lead wave asymmetry in *Waves Tonya* and *Wyatt* and their subsequent evolution through the critical point is consistent with that described above for *Wave Sonny*. We summarize the attributes of the evolution process for each of the wave groups in Figs. 7 and 8. The speed of each wave group's front edge shows a clear departure from that of the trough and rear edge (Figs. 7a–c). This separation continued as the waves approached their respective critical points. In each case the front of the wave traveled $\sim$5 cm s^{-1} faster than the trough/rear of the wave. The increased speed of the front edge marks the onset of the structural asymmetry in the waves. The asymmetry continued to develop as the speed of the front remains greater than that of the rest of the wave. Note that for each wave this pattern of asymmetry onset and further development is present. Wave speed estimates given in Fig. 2 appear inconsistent with values shown in Fig. 7; however, the two are resolved if the average wave speed is calculated using all locations along wave transits.

The evolution of the asymmetry in the lead waves is quantified using the wave slope of the front and rear faces (Fig. 8). Slope magnitudes were calculated using a linear fit to an acoustic backscatter contour associated with the pycnocline. (The front and rear faces are fit separately using a least squares approximation to a line.) This technique depends on the premise that density surfaces follow backscatter contours. For the waves presented here, this assumption seems reasonable (Fig. 4a). For *Wave Sonny* (Fig. 8a), the slope of the front face

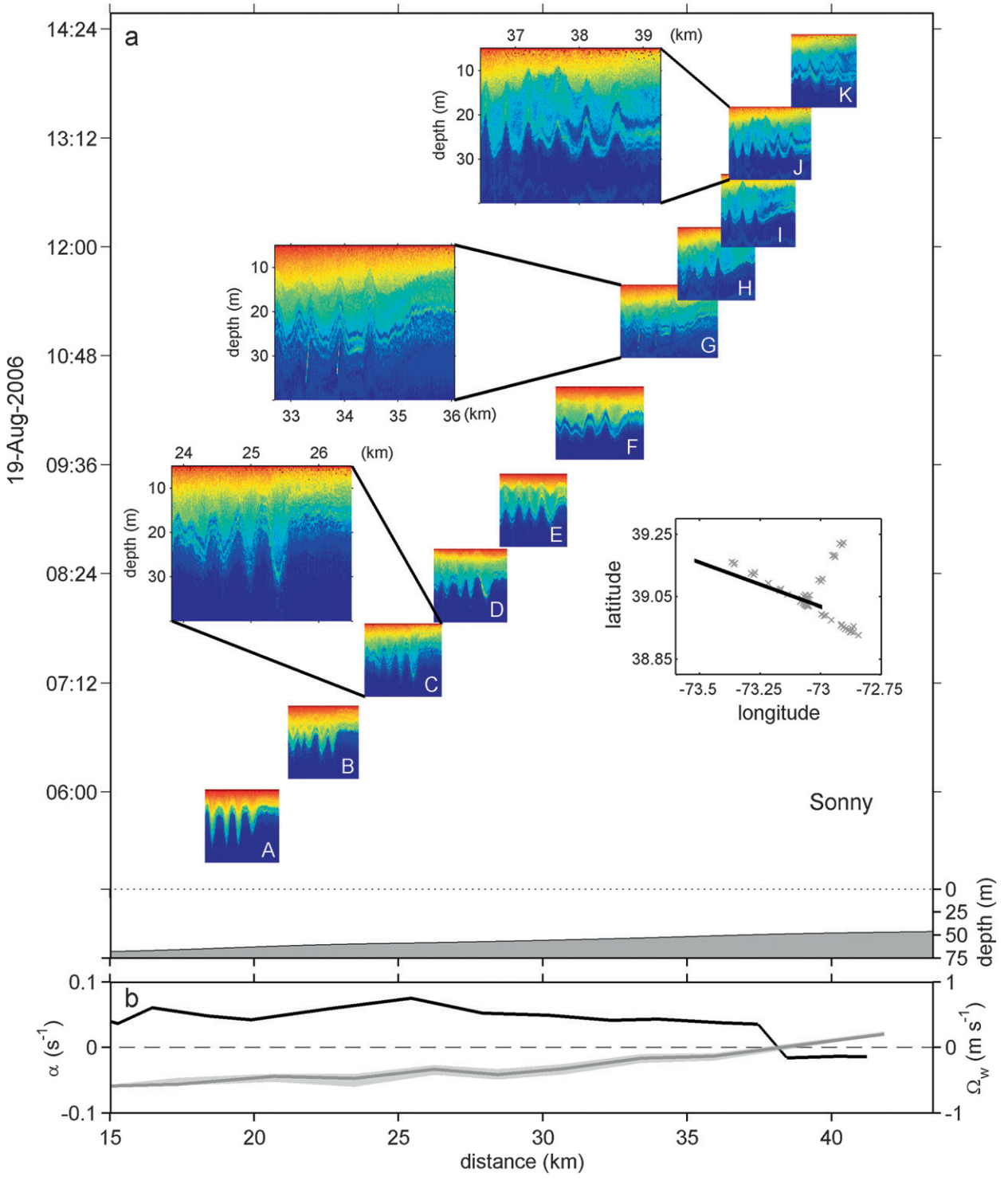

FIG. 6. (a) Acoustic backscatter transects taken perpendicular to wave front for *Wave Sonny*. Each series has been corrected for Doppler shifting so that waves may be viewed in a spatial frame with minimal distortion. (a)–(k) The horizontal axes are accurately scaled to the distance axis and the vertical axes are centered about the time of the lead wave. Select transects are enlarged in order to highlight details of structural evolution. For reference purposes, water column depth is plotted at the bottom. The lower right inset shows mooring array and approximate wave path (black line). (b) Here α is plotted in gray on the left-hand side, and Ω_w is plotted in black on the right-hand side.

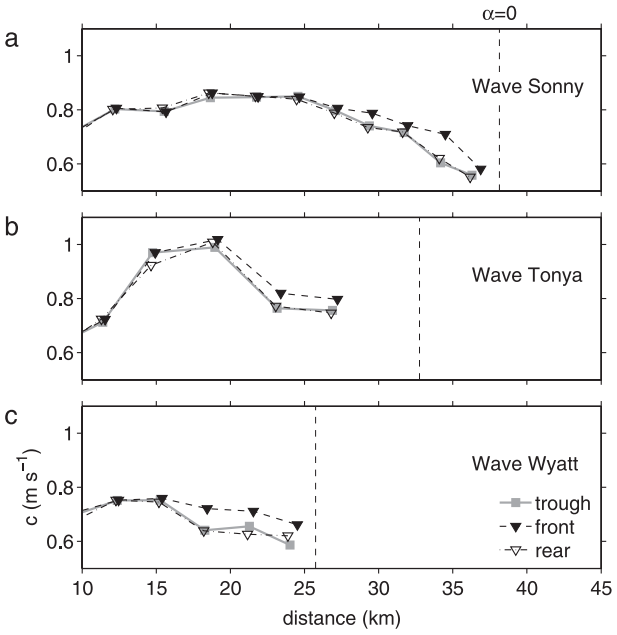

FIG. 7. Wave speed of the front edge (solid triangles), trough (gray squares), and rear edge (open triangles) for *Waves* (a) *Sonny*, (b) *Tonya*, and (c) *Wyatt*. Only wave speeds associated with depression waves are shown. The critical point ($\alpha = 0$) is marked with the vertical dashed line.

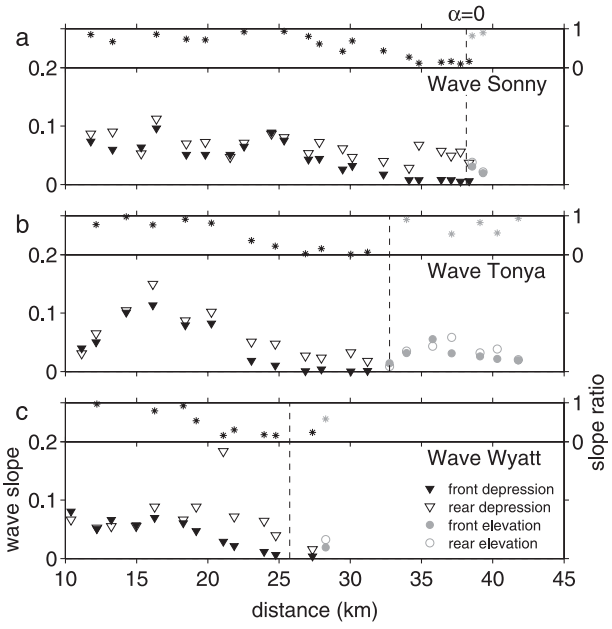

FIG. 8. (left) Slope magnitude of front (solid markers) and rear face (open markers) for *Waves* (a) *Sonny*, (b) *Tonya*, and (c) *Wyatt*. Black triangles represent waves of depression, and gray circles represent waves of elevation. (right) The ratio of the front slope to the rear slope (*). The critical point ($\alpha = 0$) is marked with the vertical dashed line.

tended to zero as the wave approached the critical point. An increase in the rear slope is observed at approximately 34 km (i.e., the rear face steepened), after which the rear slope remained relatively constant. The shift from symmetric waves to asymmetric waves is emphasized in the slope ratio. Prior to transition the ratio is near 1; through the transitional period, this ratio decreases steadily toward 0. After transition lead elevation waves (gray markers) are once again nearly symmetric, as the front slope of the elevation wave now corresponds to rear slope of the depression wave just prior to transition. A similar pattern is observed for *Tonya* (Fig. 8b) and *Wyatt* (Fig. 8c). *Wave Tonya* displayed a steady decrease toward zero in the front slope, while the rear slope remained greater than zero and fairly steady. After transition, symmetric elevation waves (slope ratio = 1) were observed for a considerable distance (over 10 km). For *Wave Wyatt* the large asymmetry apparent at 21 km stands out as an anomaly. The rear face was extremely steep, possibly approaching the breaking limit documented by Vlasenko and Hutter (2002). However, an analysis of their breaking criterion reveals that the mild slope dominated, and topographically controlled breaking was highly unlikely. The slope of the front face continued to weaken past this point. While a decrease is also apparent in the slope of the rear face, the slope ratio nevertheless tends to zero, mirroring the development in the other two wave groups.

The transition from depression to elevation waves is clear (Fig. 9). In each case, the theoretical critical point, $\alpha = 0$, predicts the observed transition to elevation waves as defined by Ω_w. Figure 9a is an exact replication of Fig. 6b for *Sonny* and has been discussed previously. For *Wave Tonya* (Fig. 9b) the lead elevation wave emerged past 34 km. As with *Sonny*, the observed transition ($\Omega_w = 0$) is in good agreement with the predicted critical point ($\alpha = 0$). The wave group was transited several times beyond this point, and the elevation wave structure was clearly developed. Both *Sonny* and *Tonya* displayed a smooth transition of background conditions from a depression- to elevation-friendly environment. In contrast, the background conditions for *Wave Wyatt* were more complex (refer to Fig. 3), and as may be expected the shoaling process is not as clear. Around 28 km the signature of the initial depression wave is faint; a weak positive vorticity (not shown) precedes a relatively stronger negative vorticity, which seems to support the impending demise of the lead depression wave and emergence of an elevation wave. Recall, however, that the background conditions for *Wave Wyatt* hovered around $\alpha = 0$ rather than clearly transitioning. Similarly, the wave form disintegrated into a disorganized assortment

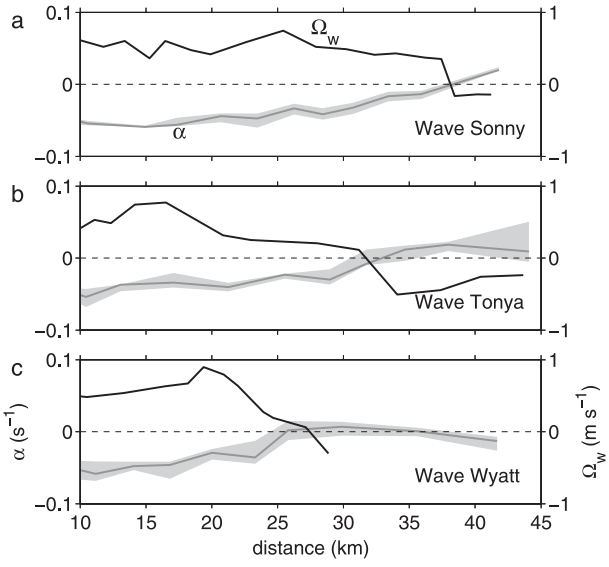

FIG. 9. The extrema of Ω_w (black lines, rhs) and α (gray lines, lhs) for *Waves* (a) *Sonny*, (b) *Tonya*, and (c) *Wyatt*.

of disturbances of the pycnocline past this point rather than clearly establishing a lead elevation wave, and we cease to recognize a leading wave of either polarity shoreward of this region.

6. Summary

Observations of three groups of shoaling NLIWs of depression reveal the complex evolution of each of the leading waves. Shoaling is controlled by background stratification and velocity, which vary not only for each of the wave trains, but also over the shoaling duration for a particular train that in each case is longer than either a tidal cycle or inertial period. As the waves traveled shoreward, they experienced a decrease in water column depth, an increase in pycnocline depth, and a change in background shear. These factors all contributed to the development of a critical point, where conditions change from supporting depression waves to supporting elevation waves.

As the waves approached the theoretical critical point ($\alpha = 0$) an asymmetry developed in the lead wave; the front edge accelerated relative to the trough and rear edge, leading to a broadening of the front face while the rear face of the wave remained steep. Eventually, the slope of the front face of the lead depression wave became indistinguishable from zero. At this point an elevation wave, formed by combining the rear face of the original depression wave with the front face of the second wave in the train, emerged as the leading wave. The signature of transition is apparent in the wave's vertical velocity and vorticity. For a depression wave, downwelling precedes upwelling as horizontal velocity converges at the leading edge of the wave near the surface. Furthermore, the wave-induced circulation yields a positive vertically integrated wave vorticity through a depression wave. The reverse is true for elevation waves. This difference is utilized to establish a diagnostic for the observed wave transformation. For each of the wave groups, the observed transition point coincides with the prediction from small-amplitude wave theory, as long as the effect of background shear is included. For two of the three waves this transition is clearly defined; for the third, background conditions produce a situation that appears favorable to neither elevation nor depression waves.

Acknowledgments. This work was funded by the Office of Naval Research. We are grateful to the captain, crew, and marine technician of R/V *Oceanus*. We acknowledge the assistance of Mike Neeley-Brown, Ray Kreth, Alexander Perlin, Greg Avicola, and Sam Kelly in obtaining the data. This work has benefited greatly from discussions with Bill Smyth.

REFERENCES

Bogucki, D., T. Dickey, and L. G. Redekopp, 1997: Sediment resuspension and mixing by resonantly generated internal solitary waves. *J. Phys. Oceanogr.,* **27,** 1181–1196.

Grimshaw, R., E. Pelinovsky, T. Talipova, and A. Kurkin, 2004: Simulation of the transformation of internal solitary waves on oceanic shelves. *J. Phys. Oceanogr.,* **34,** 2774–2791.

Helfrich, K. R., and W. K. Melville, 1986: On long nonlinear internal waves over slope-shelf topography. *J. Fluid Mech.,* **167,** 285–308.

——, ——, and J. W. Miles, 1984: On interfacial solitary waves over slowly varying topography. *J. Fluid Mech.,* **149,** 305–317.

Klymak, J. M., and J. N. Moum, 2003: Internal solitary waves of elevation advancing on a shoaling shelf. *Geophys. Res. Lett.,* **30,** 2045, doi:10.1029/2003GL017706.

Lamb, K. G., 1997: Particle transport by nonbreaking internal solitary waves. *J. Geophys. Res.,* **102,** 18 641–18 660.

——, 2003: Shoaling solitary internal waves: On a criterion for the formation of waves with trapped cores. *J. Fluid Mech.,* **478,** 81–100.

Liu, A. K., Y. S. Chang, M.-K. Hsu, and N. K. Liang, 1998: Evolution of nonlinear internal waves in the East and South China Seas. *J. Geophys. Res.,* **103,** 7995–8008.

Moum, J. N., and W. D. Smyth, 2006: The pressure disturbance of a nonlinear internal wave train. *J. Fluid Mech.,* **558,** 153–177.

——, M. C. Gregg, R. C. Lien, and M. E. Carr, 1995: Comparison of turbulence kinetic energy dissipation rate estimates from two ocean microstructure profilers. *J. Atmos. Oceanic Technol.,* **12,** 346–366.

——, D. M. Farmer, W. D. Smyth, L. Armi, and S. Vagle, 2003: Structure and generation of turbulence at interfaces strained by internal solitary waves propagating shoreward over the continental shelf. *J. Phys. Oceanogr.,* **33,** 2093–2112.

——, ——, E. L. Shroyer, W. D. Smyth, and L. Armi, 2007: Dissipative losses in nonlinear internal waves propagating across the continental shelf. *J. Phys. Oceanogr.,* **37,** 1989–1995.

Osborne, A. R., and T. L. Burch, 1980: Internal solitons in the Adaman Sea. *Science,* **208,** 451–460.

Pineda, J., 1994: Internal tidal bores in the nearshore: Warm-water fronts, seaward gravity currents and the onshore transport of neustonic larvae. *J. Mar. Res.,* **52,** 427–458.

Sandstrom, H., and J. A. Elliott, 1984: Internal tide and solitons on the Scotian shelf: A nutrient pump at work. *J. Geophys. Res.,* **89,** 6415–6426.

——, and N. S. Oakey, 1995: Dissipation in internal tides and solitary waves. *J. Phys. Oceanogr.,* **25,** 604–614.

Scotti, A., and J. Pineda, 2004: Observation of very large and steep internal waves of elevation near the Massachusetts coast. *Geophys. Res. Lett.,* **31,** L22307, doi:10.1029/2004GL021052.

Tang, D. J., and Coauthors, 2007: Shallow water '06. *Oceanography,* **20,** 156–167.

Vlasenko, V., and K. Hutter, 2002: Numerical experiments on the breaking of solitary internal waves over a slope-shelf topography. *J. Phys. Oceanogr.,* **32,** 1779–1793.

——, and N. Stashchuk, 2007: Three-dimensional shoaling of large-amplitude internal waves. *J. Geophys. Res.,* **112,** C11018, doi:10.1029/2007JC004107.

Zhao, Z., V. V. Klemas, Q. Zheng, and X.-H. Yan, 2003: Satellite observation of internal solitary waves converting polarity. *Geophys. Res. Lett.,* **30,** 1988, doi:10.1029/2003GL018286.